applied sciences

MDPI

Article

Structure-Dependent Electrochemical Behavior of 2-Pyridone Derivatives: A Combined Experimental and Theoretical Study

Aleksandra Mašulović [1], Jelena D. Lović [2,*], Jelena Lađarević [3,*], Vesna Vitnik [4], Željko Vitnik [4], Milka Avramov Ivić [2] and Dušan Mijin [3]

[1] Innovation Centre of the Faculty of Technology and Metallurgy, University of Belgrade, Karnegijeva 4, 11000 Belgrade, Serbia; amasulovic@tmf.bg.ac.rs
[2] Department of Electrochemistry, Institute of Chemistry, Technology and Metallurgy, University of Belgrade, Njegoševa 12, 11000 Belgrade, Serbia; milka@tmf.bg.ac.rs
[3] Faculty of Technology and Metallurgy, University of Belgrade, Karnegijeva 4, 11000 Belgrade, Serbia; kavur@tmf.bg.ac.rs
[4] Department of Chemistry, Institute of Chemistry, Technology and Metallurgy, University of Belgrade, Studentski Trg 12-16, 11000 Belgrade, Serbia; vesnak@chem.bg.ac.rs (V.V.); zvitnik@chem.bg.ac.rs (Ž.V.)
* Correspondence: jelena.lovic@ihtm.bg.ac.rs (J.D.L.); jmirkovic@tmf.bg.ac.rs (J.L.)

Abstract: In this work, the electrooxidation ability of nine pyridones was evaluated using cyclic (CV) and square-wave voltammetry (SWV) in Britton–Robinson (BR) aqueous buffer solutions on a glassy carbon electrode (GC). The dependence of electrochemical activity on pyridone structure was elucidated by means of experimentally obtained spectra and quantum chemical calculations. Firstly, it was shown that electrochemical activity is determined by the –OH group as a substituent in position 6 of the pyridone ring. By coupling the experimentally obtained UV-Vis spectra and DFT calculations, the most stable forms, both protonated and deprotonated, were defined. The calculated values are consistent with the electrochemical behavior observed, indicating that the deprotonated anionic form was the most electrochemically active. Moreover, the impact of the substituent in position 3 of the pyridone scaffold was discussed.

Keywords: 2-pyridones; cyclic voltammetry; square-wave voltammetry; DFT calculations; electrooxidation

Citation: Mašulović, A.; Lović, J.D.; Lađarević, J.; Vitnik, V.; Vitnik, Ž.; Avramov Ivić, M.; Mijin, D. Structure-Dependent Electrochemical Behavior of 2-Pyridone Derivatives: A Combined Experimental and Theoretical Study. *Appl. Sci.* **2023**, *13*, 10276. https://doi.org/10.3390/app131810276

Academic Editor: Diego Centonze

Received: 18 July 2023
Revised: 4 September 2023
Accepted: 6 September 2023
Published: 13 September 2023

1. Introduction

Nowadays, due to their diverse reactivity, pyridones have arisen as prominent constituents of various natural products and privileged pharmacophores in drug discovery [1]. 2-pyridones (2-hydroxypyridine) and their derivatives represent a valuable *N*-heterocyclic building block of molecules with remarkable antibacterial [2,3], antifungal [4], anti-inflammatory [5], antiviral [6] and anticancer [7] activities. In 2020, a 2-pyridone-based tazemetostat (TazverikTM) was approved by the U.S. Food and Drug Administration as a drug for the treatment of epithelioid sarcoma, the first drug of its kind to inhibit the EZH2 enzyme [8]. The latest findings have identified 13 natural products containing 2-pyridone rings as inhibitors of the SARS-CoV-2 main protease, making them promising candidates in the treatment of COVID-19 [9]. Furthermore, 2-pyridone structures have emerged as suitable ligands in transition metal catalysis [10]. These compounds gain attention in technology-driven research areas due to their potential application in electronic organic devices, replacing traditional inorganic semiconductors [11]. Owing to the latest successes of 2-pyridone-based compounds in different fields, the chemistry of this valuable heterocyclic ring represents an important subject for future research and the development of new, more efficient compounds.

In recent years, significant progress has been made in electroanalytical techniques for the detection of heterocyclic compounds of biological significance [12–14]. Moreover,

the use of theoretical calculations is often employed along with experimental results in order to highlight the structure–electrochemical properties relationship and define the origin of electrochemical stability [15–17]. Although the physicochemical properties of the 2-pyridone ring have been studied extensively, reports on their electrochemical behavior are rare, hence the development of selective electrochemical sensors for their sensitive and selective detection.

Among these, an electrochemical reduction of 1-benzylideneamino-4,6-diphenyl-2-pyridone and 1-amino-4,6-diphenyl-2-pyridone was conducted in an ethanolic BR buffer by applying polarography, CV with a hanging mercury drop electrode and controlled-potential electrolysis with a mercury pool electrode [18,19]. Moreover, an electrochemical reduction of aldimines derived from 1-amino-4,6-diphenyl-2-pyridone and 1-benzylideneamino-4,6-diphenyl-2-pyridone in an ethanolic BR buffer was studied [18], as well as an electrochemical reduction of l-amino-4,6-diphenyl-2-pyridone in an ethanolic buffer [19].

Although the oxidation of 2-pyridones has not been studied, a series of variously substituted 5-carboxy-6-methyl-3,4-dihydro-2(1H)-pyridone derivatives were electrochemically oxidized on a GC electrode, in a non-aqueous electrolyte, dry acetonitrile, by means of CV measurements. It was shown that all the investigated 3,4-dihydropyridones underwent irreversible oxidation and that their derivatives were electrochemically oxidized to 2-pyridones, involving the removal of 2 electrons and 2 protons, which was confirmed by single crystal X-ray crystallography [20]. Also, the method of platinum electrodes by means of a rotating ring-disk electrode (RRDE) has been used for electrochemical oxidation of substituted 3,4-dihydro-2-pyridones in anhydrous acetonitrile, wherein they were characterized by kinetic parameters. It was shown that the first stage of the electrochemical oxidation of substituted 3,4-dihydro-2-pyridones corresponds to a two-electron process leading to the formation of the corresponding substituted 2-pyridones [21]. On the other hand, the electrooxidation of pyridones in aqueous electrolytes has not been studied so far.

Considering the importance of 2-pyridone derivatives in various fields and encouraged by all the above statements, this work focused on the electrooxidation ability of nine pyridones (**1**–**9**, Figure 1) using CV and SWV in BR aqueous buffer solutions on a GC electrode. As many of the biologically active compounds contain a pyridone scaffold, electroanalytical techniques are useful tools for the characterization, consideration of application purposes, as well as for the detection of small quantities of the compounds in solution. Bearing this in mind, this work contains an experimental and theoretical study of the electrochemical activity of pyridones, with respect to various substituents in positions 1, 3 and 6 of the pyridone ring. DFT calculations were performed in order to support the experimental findings, wherein the most stable forms of pyridones (protonated and deprotonated) were defined and related to their electrochemical activity. Good correlations between experimental and theoretical data were established. In this study, the structural fragment responsible for electrochemical activity in the analyzed compounds was defined, revolutionizing the identification of electroactivity in future biologically active synthetic compounds and significantly advancing the field of electrochemical analysis methods for biological activity assessment. This work will furnish the essentials of the structure–property relationship and enable a general understanding of the properties affected by the nature of the compounds, thus ensuring application across diverse domains such as drug development, materials engineering and catalyst design.

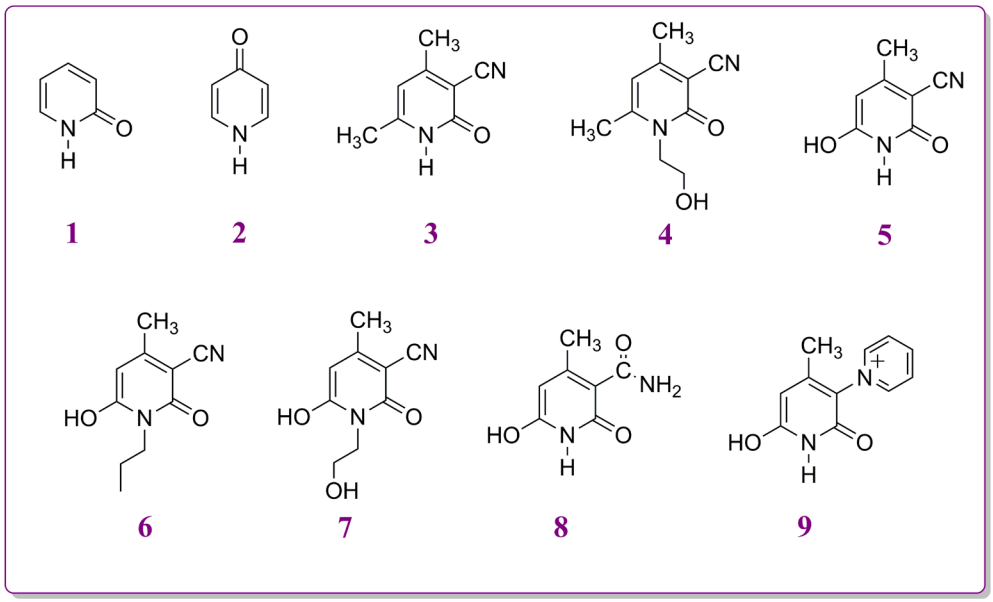

Figure 1. Structures of the investigated pyridones **1**–**9**.

2. Materials and Methods

The investigated pyridones (**3**–**9**) had previously been synthesized [22,23]. Compounds **1**, **2** as well as all chemicals used for experiments were p.a. grade (acetic acid, boric acid, phosphoric acid sodium hydroxide) and were purchased from Sigma (St. Louis, MO, USA), Merck (Darmstadt, Germany) and Acros Organics (Geel, Belgium). 18 MΩ cm deionised water was obtained from a Milipore Waters Milli-Q (Darmstadt, Germany) purification unit and was used for all experiments.

2.1. Electrochemical Measurements

All electrochemical measurements were performed using PGZ 402 Volta Lab (Radiometer Analytical, Lyon, France) by means of a three-electrode cell with a GC PINE working electrode (area 0.5 cm^2), Au wire as the auxiliary electrode, and a saturated calomel reference electrode (SCE). GC was polished with 1, 0.3 and 0.05 µm Al_2O_3 polishing powder, then rinsed with a mixture of 50% 18 MΩ cm deionized water and 50% concentrated sulfuric acid and finally washed with deionized water. BR aqueous universal buffer solutions and supporting electrolytes were deoxygenated by purging with nitrogen. In order to ensure a proper pH value for the experiments, BR buffer solutions were prepared by mixing appropriate amounts of acetic acid, boric acid, phosphoric acid and 0.2 M sodium hydroxide solutions [24,25]. The concentration of the investigated compounds in the buffered media for the electrochemical experiments was 5×10^{-4} mol dm^{-3}. Besides CV measurements scanned at a scan rate of 50 mV s^{-1}, SWV was also performed. The optimized parameters of SWV were as follows: accumulation time 2 s at E = −0.4 V (SCE); step size 5 mV; pulse size 25 mV; frequency 2 Hz; and scan rate 1 mV s^{-1}.

2.2. UV-Vis Measurements

Ultraviolet-visible (UV-Vis) absorption spectra were recorded on a Shimadzu 1700 spectrophotometer (Shimadzu, Kyoto, Japan). Water solutions of investigated pyridones were from 210 to 650 nm at room temperature. Moreover, UV-VIS spectroscopy was used to determine the pKa value of **9** according to the procedure described in literature [26].

2.3. Method of Calculation

All DFT calculations were performed using a Gaussian 09 molecular package [27] using the B3LYP [28] and M06-2X [29] methods in combination with the 6-311++G(d,p) basis set [30,31]. The initial geometry generated from standard geometrical parameters was

minimized without any constraint in potential energy surface and with default convergence criteria. For the optimization of the radical species, an unrestricted approach was applied. The optimized structures were confirmed to be real minima by frequency calculation (no imaginary frequency).

The solvent effects of water were taken into account with a conductor-like polarizable continuum model (CPCM) [32] through a reoptimization of the gas-phase geometries of all investigated species. The absorption spectra of pyridones were simulated using the TD-DFT method with water as a solvent.

To understand the role played by the differences between the structural and electronic features of these molecules, the following properties were calculated: (1) the energy of the highest occupied molecular orbital (HOMO); (2) the energy of the lowest unoccupied molecular orbital (LUMO); (3) vertical (VIE) and adiabatic (AIE) ionization energies.

For an electrochemical oxidation reaction where the pyridone is in the protonated or deprotonated molecular form P with net charge n, the reaction is presented as follows:

$$P^n - e^- \rightarrow R^{n+1} + \Delta E_{ox}$$

where ΔE_{ox} can be represented as vertical (VIE) or adiabatic (AIE) ionization energies.

The electrooxidation reaction is mimicked using these two approaches, starting from a fully optimized pyridone molecule/ion (initial state) [33]:

1. Vertical transition of pyridone molecular form, where the final state preserves the geometry of the initial state:

$$VIE = E_0\ (R^{n+1}) - E_0\ (P^n) \quad (1)$$

where VIE represents vertical ionization energy, E_0 (R^{n+1}) is the energy of the pyridone radical (oxidated state) with preserved geometry of the optimized pyridone form in its initial state, and E_0 (P^n) is the energy of the optimized pyridone form in its initial state.

2. Adiabatic transition of the pyridone molecular form where the final radical state is energetically relaxed to its minimum:

$$AIE = E_0\ ({R_{opt}}^{n+1}) - E_0\ (P^n) \quad (2)$$

where AIE is adiabatic ionization energy, E_0 (${R_{opt}}^{n+1}$) is the energy of the optimized pyridone radical (oxidated state), and E_0 (P^n) is the energy of the optimized pyridone form in initial state.

3. Results and Discussion

3.1. Pyridones: UV-Vis and Electrochemical Measurement Perspective

Since findings on the electrochemical behavior of pyridone derivatives are scarce in the literature, we thereby selected compound **9** due the peculiarity of its structure. The synthesis of **9** was reported earlier [34] and its crystal structure was revealed in our previous work [23]. Namely, **9** was proven to exist in a deprotonated zwitter-ionic form in the solid state (Figure 2) [23]. On the other hand, in solutions, this compound exists in an equilibrium of its zwitter-ionic and protonated forms (Figure 2). The relative ratio of the forms depends on the pH value of the solution, favoring the protonated form in an acidic and the zwitter-ionic one in an alkaline medium. It should be pointed out that the protonated form is positively charged, while the zwitter-ionic form is formally neutral. Namely, by UV-Vis spectrophotometric titration, the pKa value of compound **9** was calculated to be 3.5. Below this calculated value, the positively charged protonated form (Figure 2) is dominant, wherein above a pH value of 3.5, the ratio of the zwitter-ionic form increases. The stated can be seen from the UV-Vis spectra in Figure 2, wherein at pH 1.81, the peak at 315 nm is ascribed solely to the protonated form. On the other hand, the increment in the ratio of the zwitter-ionic form can be evidenced by the appearance of a shoulder (pH values 2.66 and 3.03) and later of a peak at 390 nm, when the pH value

increases above pKa. The emergence of the new peak is followed by bathochromic shift of the dominant peak at lower wavelengths.

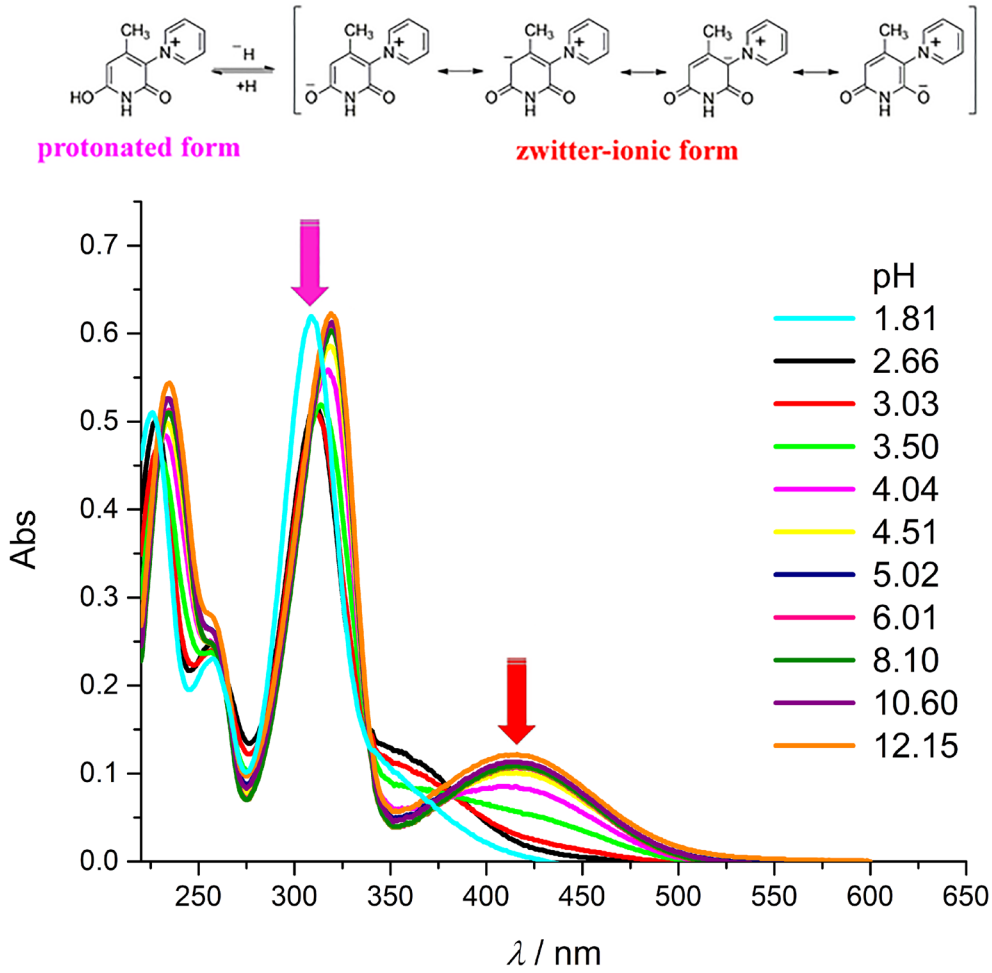

Figure 2. UV-Vis spectra of pyridone **9** at different pH values, obtained by titration using drops of NaOH and HCl solutions with designated structures of protonated and deprotonated forms.

Furthermore, to elucidate the electrochemical activity–structure relationship, bearing in mind the pH dependency of compound **9**, CVs were recorded in a BR electrolyte with pH varying from 1.81 to 11.98. Forward scans of the CVs are shown in Figure 3. Arrows in Figure 3 depict a trend following the pH value increase. In an acidic medium (pH = 1.81–6.4), peak current values obtained for the oxidation of **9** decrease with the increase of the pH value, the highest value being 107 μA cm^{-2} for pH 1.81. In an alkaline medium (pH = 8.79–11.98), the reaction currents increase with the rise in pH up to 130 μA cm^{-2}. The increase in pH value shifts the peak potential (Ep) in a negative direction. Considering the above, as well as the fact that the structure of **9** is pH-dependent (Figure 2), the involvement of protons in the electrooxidation of **9** can be assumed. Previously reported data on the pH-dependent oxidation of organic compounds show that the deprotonation reaction occurs during the oxidation process [35]. The peak potential of compound **9** correlates linearly with pH value (inset in Figure 3), with a linear regression equation of Ep(mV) = −28.85 pH + 986.02 (R^2 = 0.992). The calculated slope of 28.8 mV/pH is very close to the Nernst value of a two-electron and one-proton process [35]. According to this, a putative electrochemical oxidation mechanism is presented in Figure S2 (Supplementary Materials) in correspondence to data found in the literature [36].

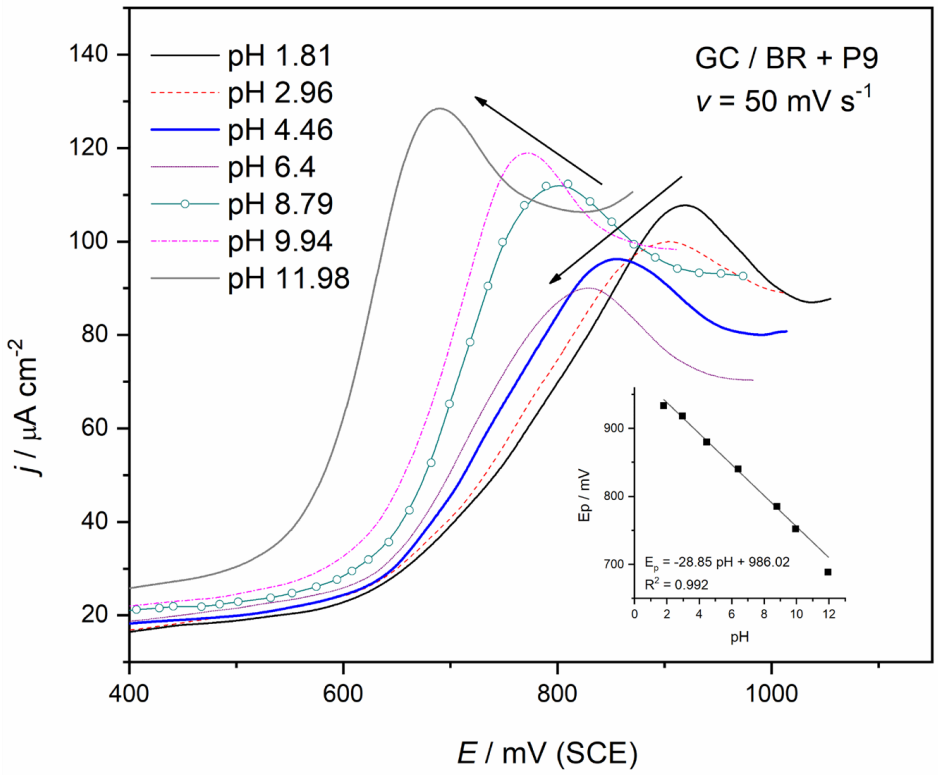

Figure 3. Forward scan of CVs of 5×10^{-4} M **9** in BR buffer at v = 50 mV s^{-1}, T = 295 K. Inset: Correlation between peak potential of compound **9** and pH value.

In order to reveal the structural fragment responsible for the oxidation of **9**, pyridones **1**–**8** were systematically chosen for further CV experiments (Figure S1, Supplementary Materials). Firstly, **1** and **2** were used as examples of unsubstituted pyridones and were inactive in the BR buffer over the investigated pH range, indicating that neither the amide fragment (NH–C=O) nor the separated –C=O and –N–H groups could be solely responsible for the electrochemical activity in **9**. Next, substituted pyridones (**3**–**8**) were chosen with different substituents in positions 1, 3 and 6. Pyridones with a methyl group in position 6 of the pyridone ring (**3** and **4**) did not show activity in BR buffer, while pyridones with a –OH group in position 6 were electrochemically active (**5**–**8**). This implies that electrooxidation is in close relationship with the presence of the –OH group in position 5 of pyridones **5**–**9**.

The effect of substituents on **5**–**9** was further examined in terms of their relevance and contribution to electrooxidation activity. SWV measurements were performed since this method usually shows more apparent peak currents compared to CVs [37]. In addition, the position of Ep overlaps in CV and SWV measurements. SWVs of pyridones **5**–**9** containing a –OH group in position 6 of the ring in the BR electrolyte with pH 1.81 and pH 9.94 are presented in Figure 4a,b and Table S1, considering E_p and j_p values. The first peak appearing at 0.2 V in an acidic solution and −0.2 V in an alkaline solution originated from the GC electrode in a blank solution (dotted line), as well as the currents attributed to those peaks observed in the presence of the examined pyridones. For further analysis, peaks at E > 0.5 V were considered since they corresponded to the oxidation of pyridone derivatives. By comparing the results shown in Figure 4, it can be noticed that reaction currents were higher in alkaline media and that all examined molecules exhibited a shift in peak potential towards less positive values with regard to the corresponding values obtained in an acidic medium. In addition, one well-defined voltammetric peak was established in the oxidation of pyridones **5**, **8** and **9**, while **6** and **7** exhibited two peaks. The second peak noticed in compounds **6** and **7** can be correlated with the N-substituted pyridone scaffold [38].

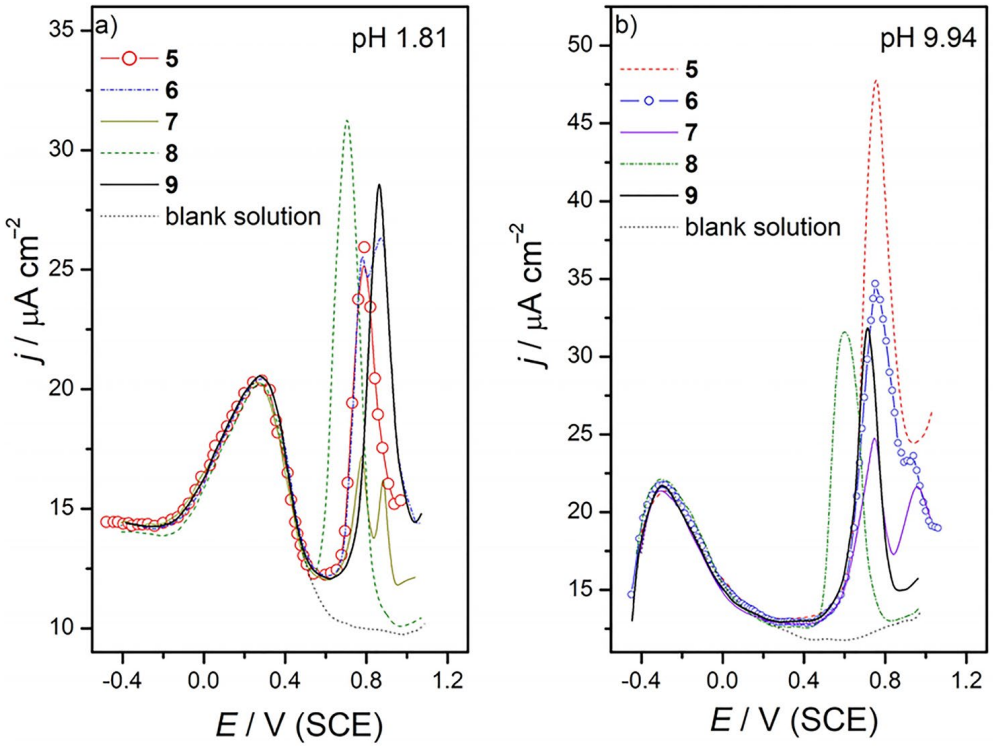

Figure 4. SWVs of the GC electrode in the presence of 5×10^{-4} M pyridones **5**–**9** in BR electrolyte with pH 1.81 (**a**) and in BR electrolyte with pH 9.94 (**b**). Accumulation time 2 s at E = −0.4 V (SCE); step size 5 mV; pulse size 25 mV; frequency 2 Hz; and scan rate 1 mV s^{-1}.

3.2. Calculated vs. Experimental: The Explanation of Electrochemical Behavior

In order to define the origin of the electrochemical activity of pyridones, it was essential to sum up their structure, bearing in mind pH dependency. DFT calculations were employed for the purpose of detailed structural characterization. Considering the presence of an acid proton present in the structure, it was expected that the examined compounds would be subjected to tautomerism and/or deprotonation depending on pH value. According to the calculations employed for pyridone **9**, more than one form was present in the solution, as depicted in Figure 5: three protonated forms (**9A**, **9B** and **9C**) and one deprotonated (**9D**) form. Moreover, the corresponding relative energies of the forms and their amounts are shown in Table 1. Corresponding geometries of the forms are provided in Supplementary Materials (Figure S3, Supplementary Materials). Calculations showed that the most stable protonated form of compound **9** corresponded to the structure protonated at C5 (**A** form), whereas the other protonated forms were present in significantly lower amounts. Considering that calculations in a vacuum gave inadequate results, they are not included in further discussion. The B3LYP method in water showed too big of a difference between **9A** and other protonated forms, whereas the stability order was consistent with calculations obtained by the M06-2X method. It is interesting to state that these calculations proved that the deprotonation of all protonated forms led to a sole anionic form, depicted by the structure of **9D**.

In order to reveal the presence of certain forms of compound **9** at different pH values, calculated UV-Vis spectra of the optimized geometries were compared with the border cases of experimentally obtained ones (pH 1.81 and pH 11.58). It was shown that peaks appearing at 210 nm and beneath overlapped with solvent absorption; therefore, the absorption peaks of **9A** and **9C** were difficult to detect in experimental UV-Vis spectra (Figure 6a). Therefore, as seen in Figure 6a, spectra obtained for compound **9** at pH 1.81 formally correspond to the optimized spectra of form **9B**. The dominant peak at 310 nm at a lower pH value shifted bathochromically to 316 nm with the rise of the pH value. Moreover, as seen in Figure 6a

(spectra **9D** and exp. pH = 11.58), the maximum rising above 350 nm, at higher pH values, can be ascribed to the deprotonated form **9D**.

Table 1. Relative energies and amounts of the most stable protonated tautomeric forms obtained with the B3LYP and M06-2X methods in water.

Form	B3LYP		M06-2X	
	E_{Rel} * (kcal mol^{-1})	ω (%)	E_{Rel} (kcal mol^{-1})	ω (%)
9A	0.00	99.33	0.00	90.63
9B	3.00	0.65	1.58	6.44
9C	5.27	0.01	2.08	2.77

* E_{Rel}—Energy relative to the most stable **9A** form.

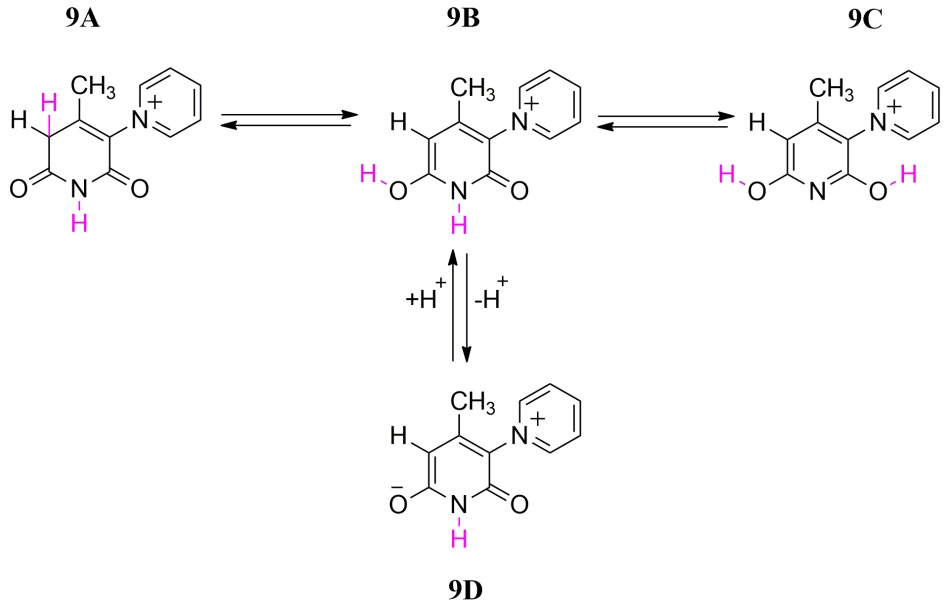

Figure 5. The most stable tautomeric forms of **9** obtained with the M06-2X/6311++G(d,p) method in water.

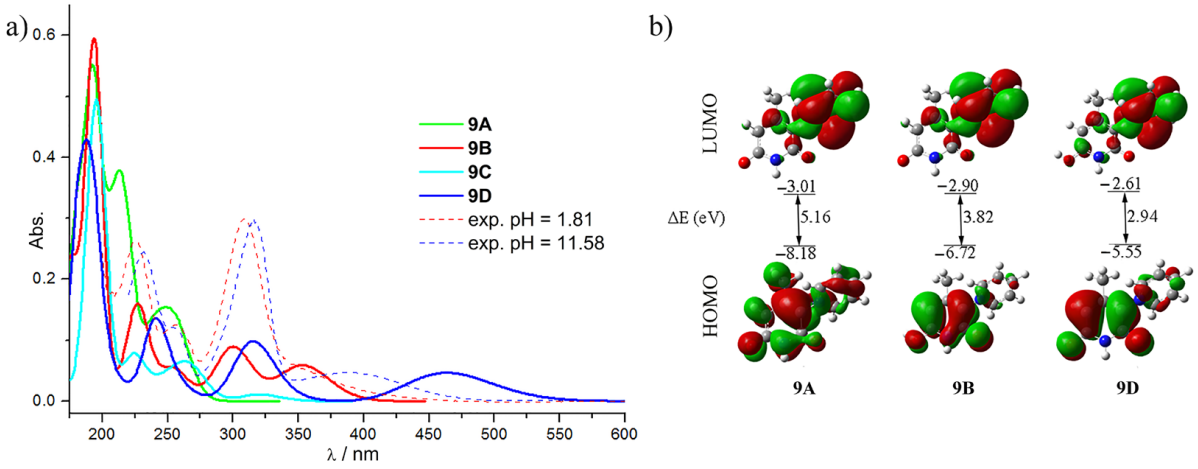

Figure 6. UV-Vis spectra in water of the calculated forms of **9** using the M06-2X/6311++G(d,p) method (full lines) along with the experimental forms (c = 5 × 10^{-5} mol dm^{-3}) at pH values 1.18 and 11.58 (dashed lines) (**a**) and distribution of frontier molecular orbitals (HOMO–LUMO) of the protonated forms of **9** (**b**).

Figure 6b depicts the distribution of frontier molecular orbitals (HOMO–LUMO) of the different forms of compound **9**, along with their energies and corresponding energy gaps. The lowest gap corresponds to **9D** (2.94 eV) which is in accordance with the UV-Vis absorption maximum of this form, which is bathochromically shifted compared to other forms of **9**. The largest energy gap can be observed for form **9A** with a corresponding absorption maximum at the lowest wavelength (250 nm). In Figure 6b, it can be observed that HOMO orbitals of forms **9B** and **9D** are mainly distributed over the pyridone ring, while in form **9A,** the HOMO orbital is dispersed over the whole molecule. The LUMO orbital of all three forms is localized over the pyridinium ring, suggesting that electron transfer occurs from the pyridone towards the pyridinium ring.

According to pH-dependent UV-Vis spectra analyses and DFT calculations, the relationship between the electrochemical behavior and the structure of compound **9** (Figure 3) is as follows: acidic media (pH 1.81, 2.96 and 4.46) favored the protonated form, and peaks emerging in CV could be ascribed mainly to the oxidation of **9A** (Figure 5). With higher pH values (pH 6.4–11.98), the share of the protonated forms decreased, whereas the reaction current increased. On the other hand, the medium at pH 11.98 contained only the deprotonated, zwitter-ionic form (**9D**). As pH values approached alkaline values, the share of **9D** increased, along with current values which were higher than those obtained for the oxidation of the protonated form. In addition, the value of the initial potential decreased, along with an increase in pH value, from 0.6 V in pH 1.81 to 0.45 V in pH 11.98, indicating an easier formation of **9D** radical. Thereby, it can be suggested that the deprotonated form was more electrochemically active than the protonated one. In other words, the share of the deprotonated form improved the electrochemical activity of compound **9**.

Moreover, DFT calculations were also employed to calculate the zero-point-corrected total energy (E0), vertical ionization energies (VIE) and adiabatic ionization energies (AIE) of the protonated and deprotonated forms of the electrochemically active pyridone **9**. VIE and AIE are energies required for the ejection of an electron, without and with a consecutive structural/conformational reorganization of the molecule, respectively [39]. These energies represent the difference between the E0 ground and E0 radical. Considering that the ratio of the **C** form of compounds **9** was negligible, the calculations obtained for this form were not taken into account. The DFT data obtained for compound **9** in water using the M06-2X method are presented in Table 2, whereas data obtained for all compounds (**5**–**8**) in gas phase and water are shown in Tables S2–S4 (Supplementary Materials).

Table 2. The vertical (VIE) and adiabatic ionization energies (AIE) in water for compound **9,** calculated with the M06-2X method.

Compound Form	E_0(radical)/Hartree	E_0(ground)/Hartree	VIE/eV	AIE/eV	ΔIE */eV
9A	–684.99165	–685.00377	8.65	8.32	0.33
9B	–685.05465	–685.06112	6.87	6.69	0.18
9D	–684.67384	–684.67969	5.58	5.42	0.16

* difference in ionization energies (VIE-AIE = ΔIE).

As seen in Table 2, the difference in the energies of the ground state and the corresponding radical is lowest in the deprotonated **9D** form, indicating that the formation of this radical is energetically the most favorable. On the other hand, the VIE of all forms is higher in value than AIE, because electron transfer is accompanied by the molecule's structural/conformational reorganization in order to achieve the most efficient electron density distribution and the most stable system. VIE and AIE energies have the lowest values for the **9D** form of the molecule, as well as the lowest difference between these values, which indicates that the anionic form of the molecule has the highest propensity to absorb excess electron density. The calculated values are in accordance with the electrochemical behavior of **9** (Figure 3), confirming that the deprotonated anionic form of **9** is in fact the most electrochemically active.

In order to compare the activity of **9** with the analogue pyridones, their structures should also be taken into account. Namely, theoretical calculations showed that pyridones **5** and **8** also exist in three protonated forms (**A**, **B** and **C**) and one deprotonated form (**D**) (Figure S4, Supplementary Materials), while the *N*-substituted one (**6** and **7**), due to the lack of proton in the nitrogen atom, may exist in two protonated forms (**A** and **B**) and one deprotonated form (**D**). The relative energies of the possible protonated forms of **5**–**8** as well as their amounts are presented in Table S5 (Supplementary Materials). According to the data obtained with the M06-2X method in water, it is clear that for all pyridones the most stable structure is that of form **A**, i.e., protonated at the C5 atom, which is analogous to **9**. Figure S5 (Supplementary Materials) depicts the experimental and calculated UV-Vis spectra of **5** in water. Good correlation between the experimentally and theoretically obtained spectra was achieved, showing that the share of protonated forms decreased with an increase in pH value. Moreover, HOMO–LUMO energies calculated for protonated form **A** and deprotonated form **D** and their distribution are presented in Figures S6 and S7 (Supplementary Materials) and Table S6 for compounds **5**–**9** in their favorable tautomeric forms.

As seen in Figure 4, among studied pyridones **5**–**9**, *N*-unsubstituted pyridone containing an amido group in position 3 of the ring (**8**) had the lowest value of peak potential in both pH values (0.7 V and 0.6 V for pH values of 1.81 and 9.94, respectively), as well as the highest peak current in an acidic medium (31.3 μA cm^{-2}). A strong correlation was found between the experimental potential values (Figure S7, Supplementary Materials) and the calculated energies (VIE, AIE, ΔIE, Tables S2–S4) of **A** forms of molecules using both calculation methods (M06-2X and B3LYP) in water, whereas the obtained correlation coefficient in gas phase was significantly lower. As for method M06-2X, a higher correlation coefficient was obtained for AIE values (R^2 = 0.948), than for VIE values (R^2 = 0.933), while as for the B3LYP method, a better correlation was obtained for VIE values (R^2 = 0.948) (Figure S8, Supplementary Materials).

Bearing in mind the above, although groups in position 3 of the pyridone ring did not directly participate in electrooxidation, they indirectly stabilized the radicals formed through their electron-accepting ability. The highest current values obtained for **8** at pH 1.81 (Figure 4a) were in accordance with the lowest energy values of 7.78 and 7.53 eV for AIE and VIE, respectively. This could be related to the lower capability of the amido group to withdraw electrons, whereas radicals were more easily formed when compared to 3-cyano (**5**, **6** and **7**) and 3-pyridinium (**9**) analogues. On the other hand, the positive charge of molecule **9** made radical formation more challenging, which was reflected in the highest potential value (0.87 V). The highest peak current value of 48 mA cm^{-2} obtained for **5** at pH 9.94 (Figure 4b) could be related to the stronger electron-withdrawing capability of the cyano group [40] which enabled the formation of deprotonated form **D** more easily with respect to **the** other 3-substituted pyridones.

The correlation coefficients of AIE and VIE (**D** form) with peak potential values in an alkaline medium were significantly lower than those obtained for protonated forms of the compounds. The obtained results were expected, considering the fact that, in the solution at pH value of 9.98, the mixture of forms **A** and **D** was present. On the other hand, SWVs indicated that all molecules were more electrochemically active in an alkaline medium, evidenced by higher current values as well as peak potentials shifts towards less positive values. This could be ascribed to the negative charge present in deprotonated molecules. Furthermore, the emergence of a second peak in SWVs of **6** and **7** could be ascribed to the oxidation of the *N*-substituted chain [35].

Figure 7 depicts electron density distribution in the formed radicals obtained for the protonated form, **A,** and the deprotonated form, **D**, of compounds **5**–**9**. As seen in Figure 7, radicals of the deprotonated forms were stabilized throughout the whole molecule by delocalization, while electron densities of radicals derived from form **A** were localized on an atom or an atomic group. This could be explained by the fact that the C5 atom of protonated form **A** was sp^3 hybridized, which prevented effective delocalization. On the other hand,

in deprotonated form **D,** all carbon atoms were sp^2 hybridized, enabling delocalization throughout the whole molecule. This indicates that the radicals of deprotonated forms were more stable, which is consistent with the obtained experimental values of current and potential. Anionic forms of the molecules exhibited a lower peak potential and higher current values in comparison to analogous protonated forms, which leads to the conclusion that they were more electrochemically active.

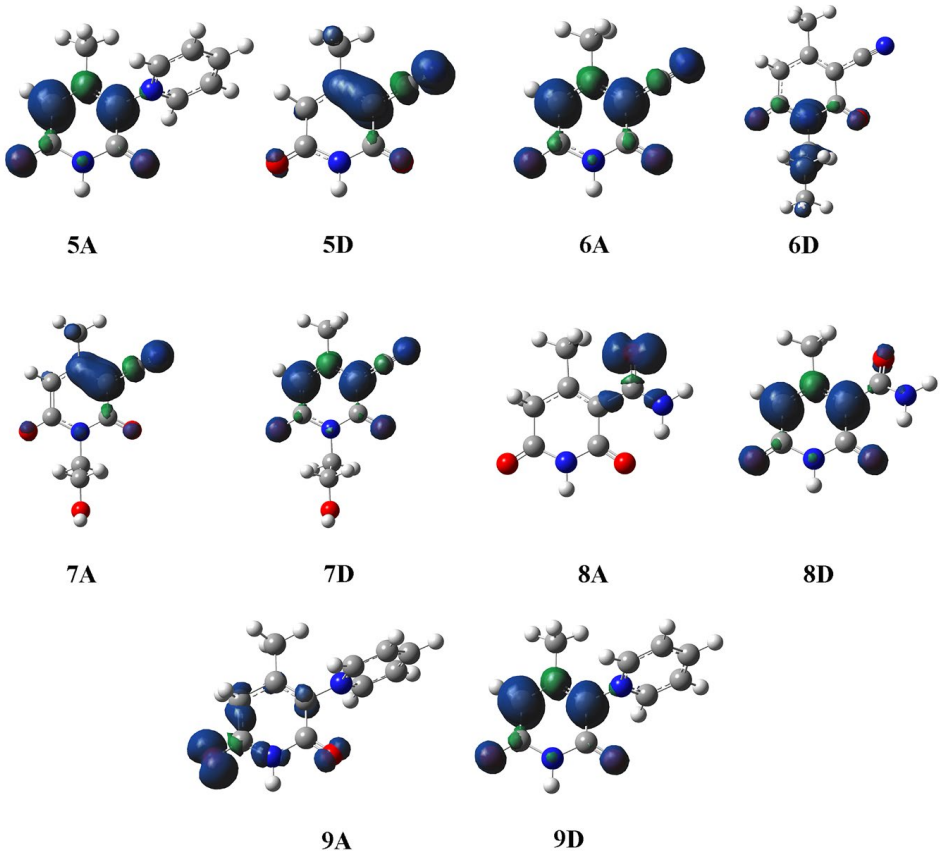

Figure 7. Distribution maps of the spin density obtained for the radicals formed in protonated form **A** and deprotonated form **D** of compounds **5**–**9**.

4. Conclusions

In this work, the electrooxidation ability of nine pyridones was evaluated using CV and SWV in BR aqueous buffer solutions on a GC electrode. The electrochemical experiments showed that the structural requirement for electrochemical activity was the presence of a hydroxyl group in position 6 of the pyridone ring. UV-Vis spectra of pyridone (**9**) containing a pyridinium substituent in position 3 indicated specific pH-dependent structures, wherein the protonated form (positively charged) was dominant in an acidic medium, while with an increase in pH value, the ratio of the deprotonated (zwitter-ionic) form increased. DFT calculations revealed that in the solution, the most stable protonated form belonged to the structure with a proton present in position 5 of the pyridone ring, while in an alkaline medium only one deprotonated form existed.

CV experiments showed that the electrochemical activity of pyridone **9** was highly affected by solution pH value. In an acidic medium, CV peaks were ascribed to the oxidation of the most stable protonated form, while in an alkaline medium, peaks originated from the oxidation of the deprotonated form**.** It is suggested that the deprotonated form was more electrochemically active than the protonated one. The experiments revealed that the electrooxidation of pyridone **9** was a two-electron and one-proton process.

SWV also indicated that the investigated molecules were more electrochemically active in an alkaline medium, evidenced by higher current values as well as peak potential shifts

towards less positive values with respect to voltammograms in an acidic medium. This was in accordance with DFT calculations suggesting that the radicals of deprotonated forms were more stable.

Although groups in position 3 of the pyridone ring did not directly participate in the electrooxidation process, they indirectly stabilized the formed radicals through their electron-accepting ability. The highest current values obtained for 3-amido-substituted pyridone in an acidic medium are ascribed to the lower capability of the amido group to withdraw electrons, wherein radicals were more easily formed when compared to 3-cyano (**5**, **6** and **7**) and 3-pyridinium (**9**) analogues. On the other hand, the positive charge in molecule **9** makes radical formation more challenging, as reflected in the highest potential value. This work will furnish the essentials of their structure–property relationship and enable a general understanding of properties affected by the nature of these compounds, thus ensuring their application across diverse domains, such as drug development, materials engineering and catalyst design.

The work in this study highlights the use of SWV and CV complemented by DFT calculations in order to define the structural fragments of 2-pyridone derivatives responsible for their electrochemical activity, representing a comprehensive framework for the characterization of the electrochemical attributes of heterocyclic compounds, namely compounds incorporating 2-pyridone fragments. This work not only advances their fundamental understanding but also enables their application across diverse domains such as drug development, materials engineering and catalyst design through tailored molecular modifications based on a profound grasp of their electronic structure–property relationship.

Supplementary Materials: The following supporting information can be downloaded at: https://www.mdpi.com/article/10.3390/app131810276/s1: Figure S1: CVs of 5×10^{-4} M 5–8 in BR buffer at v = 50 mV s^{-1}; Figure S2: A putative mechanism of the electrooxidation of compound **9**. Figure S3: The geometries of the most stable tautomers of 9 in water calculated with the M06-2X/6311++G(d,p) method; Figure S4: The geometries of the most stable tautomers of 5 in water calculated with the M06-2X/6311++G(d,p) method; Figure S5: UV-Vis spectra in water of the calculated form of 5 using the M06-2X/6311++G(d,p) method (full lines) along with the experimental form at pH values 1.18 and 11.58 (dashed lines); Figure S6: Distribution of frontier molecular orbitals (HOMO–LUMO) and their energies in protonated A form of 5–9; Figure S7: Distribution of frontier molecular orbitals (HOMO–LUMO) and their energies in deprotonated D form of 5–9; Figure S8: Correlations between obtained experimental SW peak potential and corresponding energy values (AIE and VIE) for A form of pyridones; Table S1: Electrooxidation ability of pyridones 5–9 expressed through Ep and jp at pH 1.81 and 9.94; Table S2: The vertical (VIE) and adiabatic ionization energy (AIE) in gas phase obtained with the B3LYP method; Table S3: The vertical (VIE) and adiabatic ionization energy (AIE) in water obtained with the B3LYP method; Table S4: The vertical (VIE) and adiabatic ionization energy (AIE) in water obtained with the M06-2X method; Table S5: The relative energies and shares of the most stable protonated tautomeric forms in water obtained with the B3LYP and M06-2X methods; Table S6: HOMO and LUMO energies and their gap for the most stable forms of the pyridones 5–9.

Author Contributions: Conceptualization, A.M., J.L. and D.M.; methodology, A.M., J.L., J.D.L., Ž.V. and D.M.; validation, A.M., J.L., J.D.L., M.A.I. and D.M.; formal analysis, A.M., J.L. and Ž.V.; investigation, A.M., J.D.L. and V.V.; resources, J.L., Ž.V., V.V., M.A.I. and D.M.; writing—original draft preparation, A.M., J.L., V.V. and J.D.L.; writing—review and editing, D.M., M.A.I., V.V. and Ž.V.; visualization, J.L. and A.M.; supervision, D.M. and M.A.I.; funding acquisition, J.D.L., J.L., Ž.V., M.A.I. and D.M. All authors have read and agreed to the published version of the manuscript.

Funding: This research was funded by the Ministry of Science, Technological Development and Innovation of the Republic of Serbia (RS) (Grant No. 451-03-47/2023-01/200026, 451-03-47/2023-01/200287 and 451-03-47/2023-01/200135).

Institutional Review Board Statement: Not applicable.

Informed Consent Statement: Not applicable.

Data Availability Statement: The data presented in this study are available on request from the corresponding authors or co-authors. The data are not publicly available.

Acknowledgments: This work was supported by the Ministry of Science, Technological Development and Innovation of the Republic of Serbia (RS).

Conflicts of Interest: The authors declare no conflict of interest.

References

1. Zhang, Y.; Pike, A. Pyridones in drug discovery: Recent advances. *Bioorg. Med. Chem. Lett.* **2021**, *38*, 127849. [CrossRef]
2. Li, Q.; Mitscher, L.; Shen, L. The 2-pyridone antibacterial agents: Bacterial topoisomerase inhibitors. *Med. Res. Rev.* **2000**, *20*, 231–293. [CrossRef] [PubMed]
3. Fujita, Y.; Oguri, H.; Oikawa, H. Biosynthetic studies on the antibiotics PF1140: A novel pathway for a 2-pyridone framework. *Tetrahedron Lett.* **2005**, *46*, 5885–5888. [CrossRef]
4. Fassihi, A.; Abedi, D.; Saghaie, L.; Sabet, R.; Fazeli, H.; Bostaki, G.; Deilami, O.; Sadinpou, H. Synthesis, antimicrobial evaluation and QSAR study of some 3-hydroxypyridine-4-one and 3-hydroxypyran-4-one derivatives. *Eur. J. Med. Chem.* **2009**, *44*, 2145–2157. [CrossRef] [PubMed]
5. Semple, G.; Andersson, B.; Chhajlani, V.; Georgsson, J.; Johansson, M.; Rosenquist, A.; Swanson, L. Synthesis and biological activity of kappa opioid receptor agonists. Part 2: Preparation of 3-aryl-2-pyridone analogues generated by solution- and solid-phase parallel synthesis methods. *Bioorg. Med. Chem. Lett.* **2003**, *13*, 1141–1145. [CrossRef]
6. Parreira, R.; Abrahão, O., Jr.; Galembeck, S. Conformational preferences of nonnucleoside HIV-1 reverse transcriptase inhibitors. *Tetrahedron* **2001**, *57*, 3243–3253. [CrossRef]
7. Hasvold, L.; Wang, W.; Gwaltney, S.; Rockway, T.; Nelson, L.; Mantei, R.; Fakhoury, S.; Sullivan, G.; Li, Q.; Lin, N.; et al. Pyridone-containing farnesyltransferase inhibitors: Synthesis and biological evaluation. *Bioorg. Med. Chem. Lett.* **2003**, *13*, 4001–4005. [CrossRef] [PubMed]
8. Weiss, M.; Agulnik, M. Tazemetostat as a treatment for epithelioid sarcoma. *Expert Opin. Orphan Drugs* **2020**, *8*, 311–315. [CrossRef]
9. Forrestall, K.L.; Burley, D.E.; Cash, M.K.; Pottie, I.R.; Darvesh, S. 2-Pyridone natural products as inhibitors of SARS-CoV-2 main protease. *Chem.-Biol. Interact.* **2021**, *335*, 109348. [CrossRef]
10. Wang, P.; Verma, P.; Xia, G.; Shi, J.; Qiao, J.X.; Tao, S.; Cheng, P.T.W.; Poss, M.A.; Farmer, M.E.; Yeung, K.; et al. Ligand-accelerated non-directed C–H functionalization of arenes. *Nature* **2017**, *551*, 489–493. [CrossRef]
11. Mandal, T.; Dey, A.; Pathak, S.; Islam, M.; Konar, S.; Ortega-Castro, J.; Seth, S.K.; Ray, P.P.; Frontera, A.; Mukhopadhyay, S. Structures, photoresponse properties and DNA binding abilities of 4-(4-pyridinyl)-2-pyridone salts. *RSC Adv.* **2019**, *9*, 9663–9677. [CrossRef] [PubMed]
12. Xia, Y.; Li, G.; Zhu, Y.; He, Q.; Hu, C. Facile preparation of metal-free graphitic-like carbon nitride/graphene oxide composite for simultaneous determination of uric acid and dopamine. *Microchem. J.* **2023**, *190*, 108726. [CrossRef]
13. Li, G.; Qi, X.; Wu, J.; Xu, L.; Wan, X.; Liu, Y.; Chen, Y.; Li, Q. Ultrasensitive, label-free voltammetric determination of norfloxacin based on molecularly imprinted polymers and Au nanoparticle-functionalized black phosphorus nanosheet nanocomposite. *J. Hazard. Mater.* **2022**, *436*, 129107. [CrossRef]
14. Li, G.; Wu, J.; Qi, X.; Wan, X.; Liu, Y.; Chen, Y.; Xu, L. Molecularly imprinted polypyrrole film-coated poly(3,4-ethylenedioxythiophene): Polystyrene sulfonate-functionalized black phosphorene for the selective and robust detection of norfloxacin. *Mater. Today Chem.* **2022**, *26*, 101043. [CrossRef]
15. Lin, S.; Lin, Y.; He, B.; Pu, B.; Ren, Y.; Wang, G.; Luo, Y.; Shi, S. Reclaiming Neglected Compounds as Promising Solid State Electrolytes by Predicting Electrochemical Stability Window with Dynamically Determined Decomposition Pathway. *Adv. Energy Mater.* **2022**, *12*, 2201808. [CrossRef]
16. Tufail, M.K.; Zhai, P.; Khokar, W.; Jia, M.; Zhao, N.; Guo, X. Evaluation of solid electrolytes: Development of conventional and interdisciplinary approach. *Interdiscip. Mater.* **2023**, *2*, 529–568. [CrossRef]
17. Tufail, M.K.; Zhai, P.; Jia, M.; Zhao, N.; Guo, X. Design of Solid Electrolytes with Fast Ion Transport: Computation-Driven and Practical Approaches. *Energy Mater. Adv.* **2023**, *4*, 0015. [CrossRef]
18. Martinez-Ortiz, F.; Vera, J.; Molina, P. Electrochemical behaviour of aldimines derived from 1-amino-4,6-diphenyl-2-pyridone 1-benzylideneamino-4,6-diphenyl-2-pyridone in ethanolic Britton-Robinson buffer. *J. Electroanal. Chem.* **1983**, *154*, 193–203. [CrossRef]
19. Vera, J.; Martinez-Ortiz, F.; Ripoll, A.; Molina, P. Electrochemical behaviour of l-amino-4,6-diphenyl-2-pyridone in ethanolic buffer. *Electrochim. Acta* **1986**, *31*, 1231–1233. [CrossRef]
20. Smits, R.; Turovska, B.; Belyakov, S.; Plotniece, A.; Duburs, G. Synthesis of 5-carboxy-6-methyl-3,4-dihydro-2(1H)-pyridone derivatives and their electrochemical oxidation to 2-pyridones. *Chem. Phys. Lett.* **2016**, *649*, 84–87. [CrossRef]
21. Ogle, Y.V.; Baumane, L.K.; Gavar, R.A.; Kadysh, V.P.; Stradyn', Y.P.; Lusis, V.K.; Mutsenietse, D.K.; Dubur, G.Y. Electrolytic oxidation of 2,6-dimethyl-3,5-bis(ethoxycarbonyl)-1,2-dihydropyridines in acetonitrile on platinum electrodes. *Chem. Heterocycl. Compd.* **1984**, *20*, 522–529. [CrossRef]
22. Tadić, J.; Mihajlović, M.; Jovanović, M.; Mijin, D. Continuous flow synthesis of some 6- and 1,6-substituted 3-cyano-4-methyl-2-pyridones. *J. Serb. Chem. Soc.* **2019**, *84*, 531–538. [CrossRef]

23. Mašulović, A.D.; Lađarević, J.M.; Radovanović, L.D.; Vitnik, Ž.J.; Vitnik, V.D.; Rogan, J.R.; Mijin, D.Ž. Charge assisted assembly of zwitterionic pyridone hydrates. *J. Mol. Struct.* **2021**, *1237*, 130419. [CrossRef]
24. Reynolds, J.E., III; Josowicz, M.; Tyler, P.; Vegha, R.B.; Solntsev, K.M. Spectral and redox properties of the GFP synthetic chromophores as a function of pH in buffered media. *Chem. Commun.* **2013**, *49*, 7788–7790. [CrossRef]
25. Mongay, C.; Cerda, V. A Britton-Robinson buffer of known ionic strength. *Ann. Chim. Rome* **1974**, *64*, 409–412.
26. Pandey, M.M.; Jaipal, A.; Kumar, A.; Malik, R.; Charde, S.Y. Determination of pKa of felodipine using UV–Visible spectroscopy. *Spectrochim. Acta A* **2013**, *115*, 887–890. [CrossRef]
27. Frisch, M.J.; Trucks, G.W.; Schlegel, H.B.; Scuseria, G.E.; Robb, M.A.; Cheeseman, J.R.; Scalmani, G.; Barone, V.; Mennucci, B.; Petersson, G.A.; et al. *Gaussian 09, Revision C.01*; Gaussian, Inc.: Wallingford, CT, USA, 2010.
28. Becke, A.D. Density-functional thermochemistry. III. The role of exact exchange. *J. Chem. Phys.* **1993**, *98*, 5648–5652. [CrossRef]
29. Zhao, Y.; Truhlar, D.G. The M06 suite of density functionals for main group thermochemistry, thermochemical kinetics, noncovalent interactions, excited states, and transition elements: Two new functionals and systematic testing of four M06-class functionals and 12 other functional. *Theor. Chem. Acc.* **2008**, *120*, 215–241.
30. Krishnan, R.; Binkley, J.S.; Seeger, R.; Pople, J.A. Self-consistent molecular orbital methods. XX. Basis set for correlated wavefunctions. *J. Chem. Phys.* **1980**, *72*, 650–654. [CrossRef]
31. McLean, A.D.; Chandler, G.S. Contracted Gaussian-basis sets for molecular calculations. I. Secomd row atoms, Z = 11–18. *J. Chem. Phys.* **1980**, *72*, 5639–5648. [CrossRef]
32. Barone, V.; Cossi, M. Quantum calculation of molecular energies and energy gradients in solution by a conductor solvent model. *J. Phys. Chem. A* **1998**, *102*, 1995–2001. [CrossRef]
33. Paolone, A.; Brutti, S. Comparison of the Performances of Different Computational Methods to Calculate the Electrochemical Stability of Selected Ionic Liquids. *Materials* **2021**, *14*, 3221. [CrossRef]
34. Schwarz, W.M. Colorant and Ink Compositions. U.S. Patent 5413630, 9 May 1995.
35. Vasantha, V.S.; Chen, S.-M. Synergistic effect of a catechin-immobilized poly(3,4-ethylenedioxythiophene)-modified electrode on electrocatalysis of NADH in the presence of ascorbic acid and uric acid. *Electrochim. Acta* **2006**, *52*, 665–674. [CrossRef]
36. Nady, H.; El-Rabiei, M.M.; Abd El-Hafez, G.M. Electrochemical oxidation behavior of some hazardous phenolic compounds in acidic solution. *Egypt. J. Pet.* **2017**, *26*, 669–678. [CrossRef]
37. Vajdle, O.; Šekuljica, S.; Guzsvány, V.; Nagy, L.; Kónya, Z.; Avramov Ivić, M.; Mijin, D.; Petrović, S.; Anojčić, J. Use of carbon paste electrode and modified by gold nanoparticles for selected macrolide antibiotics determination as standard and in pharmaceutical preparations. *J. Electroanal. Chem.* **2020**, *873*, 114324. [CrossRef]
38. Lucas, F.; McIntosh, N.; Jacques, E.; Lebreton, C.; Heinrich, B.; Donnio, B.; Jeannin, O.; Rault-Berthelot, J.; Quinton, C.; Cornil, J.; et al. [4]Cyclo-N-alkyl-2,7-carbazoles: Influence of the Alkyl Chain Length on the Structural, Electronic, and Charge Transport Properties. *J. Am. Chem. Soc.* **2021**, *143*, 8804–8820. [CrossRef] [PubMed]
39. Ivanov, M.V.; Wang, D.; Zhang, D.; Rathore, R.; Reid, S.A. Vertical vs. adiabatic ionization energies in solution and gas-phase: Probing ionization-induced reorganization in conformationally-mobile bichromophoric actuators using photoelectron spectroscopy, electrochemistry and theory. *Phys. Chem. Chem. Phys.* **2018**, *20*, 25615–25622. [CrossRef]
40. Tadić, J.D.; Lađarević, J.M.; Vitnik, Ž.J.; Vitnik, V.D.; Stanojković, T.P.; Matić, I.Z.; Mijin, D.Ž. Novel azo pyridone dyes based on dihydropyrimidinone skeleton: Synthesis, DFT study and anticancer activity. *Dye. Pigment.* **2021**, *187*, 109123. [CrossRef]